Spectrochimica Acta Part A 76 (2010) 137–141

Contents lists available at ScienceDirect

Spectrochimica Acta Part A: Molecular and Biomolecular Spectroscopy

journal homepage: www.elsevier.com/locate/saa

Vibrational spectra and structure of RDX and its ^{13}C- and ^{15}N-labeled derivatives: A theoretical and experimental study

Ricardo Infante-Castillo[a], Leonardo Pacheco-Londoño[b], Samuel P. Hernández-Rivera[b,*]

[a] Department of Physics-Chemistry, University of Puerto Rico-Arecibo, P.O. Box 4010, Arecibo 00613-4010, Puerto Rico
[b] Department of Chemistry, University of Puerto Rico-Mayagüez, PO Box 9000, Mayagüez 00681-9000, Puerto Rico

ARTICLE INFO

Article history:
Received 5 February 2010
Received in revised form 17 February 2010
Accepted 26 February 2010

Keywords:
RDX-^{13}C
RDX-^{15}N
Isotopomers
Ab initio force field
Vibrational analysis

ABSTRACT

Unambiguous vibrational band assignments have been made to cyclic nitramine hexahydro-1,3,5-trinitro-s-triazine, commonly known as the α-phase of RDX or α-RDX, with the use of ^{13}C and ^{15}N (on ring) enriched isotopic RDX analogues. Vibrational spectra were collected using Raman and IR spectroscopy in solid state and *ab initio* normal mode calculations were performed using density functional theory (DFT) and a 6-311G++** basis set. The calculated isotopic frequency shifts, induced by ^{13}C and ^{15}N labeling, are in very good accordance with measures ones. The changes in vibrational modes associated with the isotopic substitutions are well modeled by the calculation and previous assignments of the vibrational spectra have been revised, especially where the exact nature of the vibrational modes had been either vague or contradictory.

1. Introduction

The cyclic nitramine RDX (Royal Demolition Explosive – hexahydro-1,3,5-trinitro-*s*-triazine) is a well-known powerful secondary explosive that is commonly used in conventional munitions and various military applications. The extensive use of RDX is associated to its reasonable insensitivity to external conditions and high performance as a high explosive (HE). Various experimental [1–3] and theoretical [4–6] techniques have been used in order to determine the structure of RDX in gas, solid and liquid states. Trace explosive detection is a major technological challenge. The most promising and sensitive devices and techniques for explosive detection that provide qualitative and quantitative information are not amenable to routine field use. Some of the greatest improvements in explosives detection during the last years have been made in the area of vibrational spectroscopy. Several of these methods have been shown capable of detecting explosives on surfaces at stand-off distances [7], although much work remains to be done to improve selectivity and differentiation from matrix effects and background clutter. The interest in terahertz spectroscopy for explosive detection [8] has robustly increased.

To understand the explosive nature of RDX, the molecular structure needs to be examined in detail. RDX is known to exist in four polymorphic phases, termed α [9,10], β [11,12], γ [13–15] and δ [16]. The vibrational spectroscopy of α-RDX has been the subject of numerous studies [1–5]. However, some inconsistency exits in the available studies of α-RDX, with respect to the assignment of some normal vibrations. The α-form, shown in Fig. 1, is the stable polymorph at room temperature and is used in the general bulk level applications. The crystal structure of α-RDX was determined to be orthorhombic *Pbca* with eight molecules per unit cell [10]. The individual RDX molecules in the α-phase possess essentially C_s symmetry with two of the NO_2 groups axial and the third equatorial with respect to the triazine ring. In the present study, we have reinvestigated the structure and vibrational spectra of solid RDX in the α-phase and its ^{13}C and ^{15}N isotopomers.

Assignments of the IR and Raman bands are made mainly on the basis of empirical comparison of experimental results with those of related groups such as nitro and amino groups. There are only a few vibrations which are not combination modes involving more than one type of motion. The degree of mixing is evident in the varying amounts of frequency shifts that are observed. In this sense the effects of the ^{13}C and ^{15}N substitution on various vibrations are large enough to be useful in matching calculated and measured frequencies. The infrared and Raman spectra, in solid state, of α-phase and ^{13}C and ^{15}N (on ring) enriched RDX analogues were obtained for the study. Quantum chemical calculations have also been performed, and many vibrational bands have been clearly assigned. This work focused on the use of modern density functional theory (DFT) [17], to account for the experimental vibrational Raman and IR data from RDX and its ^{13}C- and ^{15}N-RDX isotopomers. Raman and IR frequencies were calculated at the DFT/B3LYP level using the 6-311++G** basis set. The calculated frequencies were compared

* Corresponding author. Tel.: +1 787 832 4040x3450; fax: +1 787 265 5404.
E-mail addresses: samuel.hernandez3@upr.edu, sp_hernandez_uprm@yahoo.com (S.P. Hernández-Rivera).

1386-1425/$ – see front matter © 2010 Elsevier B.V. All rights reserved.
doi:10.1016/j.saa.2010.02.051

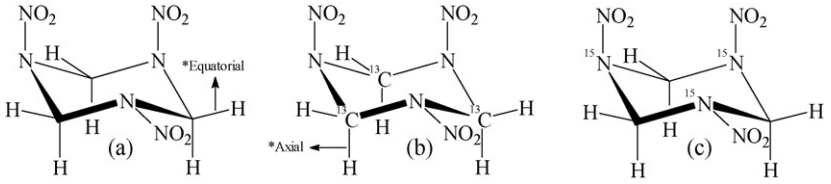

Fig. 1. Structures of (a) α-RDX; (b) $^{13}C_3$-RDX; and (c) $^{15}N_3$-RDX. *Reference for vibrational analysis.

with the experimental data and the isotopic effects are discussed. Assignments of the vibrational modes for RDX are made through comparison between experimental and density functional calculations results. The purpose of the present study is to assign the fundamental vibrational frequencies, to elucidate the structure of RDX, and to analyze the force field on the basis of IR and Raman spectra including isotopic labeling and *ab initio* force field calculations.

2. Experimental

RDX standards were obtained as 1 mg/mL solution in acetonitrile from Supelco® (Sigma–Aldrich Chemical Co., Milwaukee, WI), ^{13}C (99%) enriched RDX was obtained from Cambridge Isotope Laboratories, Inc. (Andover, MA) as 1 mg/mL acetonitrile solution and ^{15}N (99%) enriched RDX was obtained from SRI International as solid material. Acetonitrile (Sigma–Aldrich) was allowed to evaporate at room temperature after the deposition on metallic microscope slides. Fourier transform infrared (FTIR) spectra were obtained by attenuated total reflection (ATR) method in a Nexus 8700, Thermo Nicolet FTIR spectrometer in the range of 400–4000 cm^{-1}. Samples were lightly ground in preparation for placement on the ATR stage. Raman spectra were measured using a commercial Renishaw RM2000 Raman microspectrometer with vibrational and white light imaging capabilities. The 514.5 nm line of a Coherent INNOVA 308 Ar^+ ion laser system was used as the excitation source. Dispersive Raman equipment was operated in confocal mode microscopy. Spectrometers were equipped with polarization analyzers and de-scramblers. All the measurements were taken at room temperature (ca. 20 °C).

3. Computations

Ab initio density functional theory (DFT) with the B3LYP hybrid functional calculations using the Gaussian 03-W program package [18] were carried out for the α-RDX and its ^{13}C and ^{15}N isotopomers. The basis sets implemented in the program were employed without modification. The hybrid density functional B3LYP method [19,20] was used for geometry optimization, frequency location, band contours analysis and intensity calculations. In all cases, the 6-311++G** basis set was used. Frequencies for isotopically labeled RDX were recalculated following mass substitution using the force constants obtained for the most common isotope. The geometry was considered optimized yielding minimum in energy when no imaginary frequencies resulted as part of the computation. Detailed assignment was given based on the comparison between the theoretical data and the experimental results. The normal mode descriptions were obtained with the assistance of animated pictures [21] based on the normal coordinates.

4. Results and discussion

Experimental Raman and FTIR solid state spectra of RDX in its α-phase and its isotopically labeled $^{13}C_3$- and $^{15}N_3$-RDX are shown in Figs. 2 and 3. The spectra of RDX and its isotopic analogues are characterized by intense and sharp vibrational bands. Solid α-phase of RDX has close to C_s symmetry and occupies a C_1 site. The 57 fundamental vibrational modes are active in both IR and Raman. These modes included 26 planar modes with A′ symmetry and 31 non-planar modes with A″ symmetry. Several of these are not expected

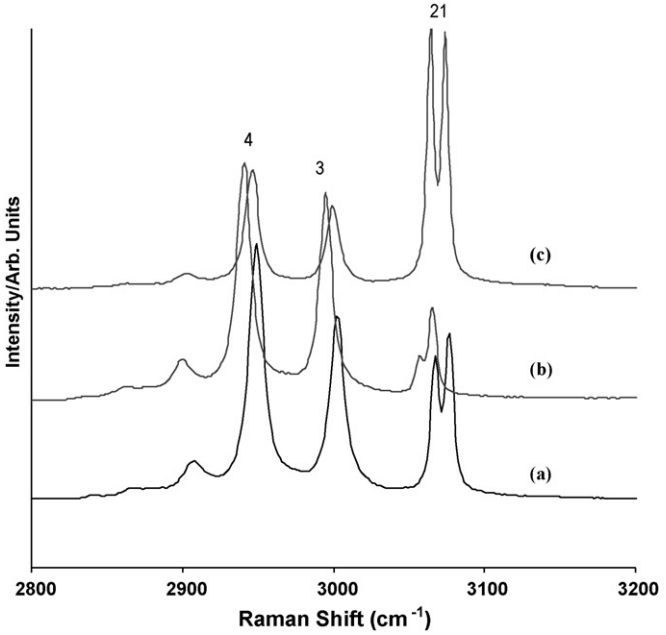

Fig. 2. Experimental FTIR spectra for RDX and isotopically labeled RDX from 500 to 1600 cm^{-1}; (a) RDX, (b) $^{13}C_3$-RDX and (c) $^{15}N_3$-RDX. Labeled peaks are explained in Table 1.

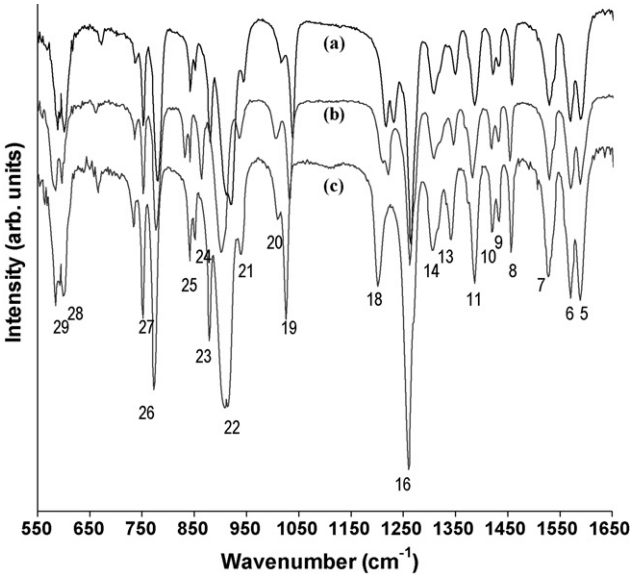

Fig. 3. Experimental Raman spectra for RDX and isotopically labeled RDX from 2800 to 3200 cm^{-1}; (a) RDX, (b) $^{13}C_3$-RDX and (c) $^{15}N_3$-RDX. Labeled peaks are explained in Table 1.

Table 1
Experimental IR and Raman vibrational signals and theoretical calculations and assignments of RDX, ^{13}C- and ^{15}N-RDX.

Mode no.	RDX			^{13}C-RDX			^{15}N-RDX			Assignment[b,c]
	IR (cm^{-1})	Raman (cm^{-1})	Calc.[a] (cm^{-1})	IR (cm^{-1})	Raman (cm^{-1})	Calc.[a] (cm^{-1})	IR (cm^{-1})	Raman (cm^{-1})	Calc.[a] (cm^{-1})	
1	3072	3076	3071	3062(−10)	3065(−11)	3061	3074(2)	3074(−2)	3070	$\nu^{as}C–H^{(Eq)}$
2	3064	3067	3065	3054(−10)	3057(−10)	3059	3064(0)	3064(−3)	3069	$\nu^{as}C–H^{(Eq)}$
3	/	3003	2953	/	2995(−8)	2950	/	2999(−4)	2957	$\nu^{as}C–H^{(Ax)}$
4	/	2949	2894	/	2941(−8)	2891	/	2945(−4)	2898	$\nu^{as}C–H^{(Ax)}$
5	1589	1594	1636	1589(0)	1594(0)	1637	1589(0)	1592(−2)	1602	$\nu^{as}NO_2^{(Ax)}$
6	1569	1573	1618	1569(0)	1572(−1)	1618	1569(0)	1569(−4)	1594	$\nu^{as}NO_2^{(Ax)}$
7	1529	1541	1592	1529(0)	1541(0)	1592	1527(0)	1537(−4)	1583	$\nu^{as}NO_2^{(Eq)}$
8	1457	1459	1472	1454(−3)	1455(−4)	1468	1456(1)	1454(−5)	1471	$\beta\ CH_2$
9	1430	1436	1445	1430(0)	1432(−4)	1442	1432(0)	1432(−4)	1444	$\beta\ CH_2$
10	1421	/	1399	1419(−2)	/	1391	1419(−2)	/	1395	$\gamma\ CH_2$
11	1386	1389	1385	1382(−4)	1383(−6)	1378	1386(0)	1385(−4)	1383	$\gamma\ CH_2$
12	/	1379	1354	/	1372(−7)	1354	/	1373(−6)	1355	$\gamma\ CH_2$
13	1348	1346	1343	1346(−2)	1345(−1)	1341	1340(−8)	1337(−9)	1342	$\nu\ N\text{-}NO_2^{(Ax)}$
14	1307	1311	1319	1309(−2)	1310(−1)	1320	1305(−2)	1305(−6)	1304	$\nu\ N\text{-}NO_2^{(Eq)}$
15	/	1275	1282	/	1272(−3)	1282	/	1269(−6)	1271	$\nu\ N\text{-}NO_2 + \gamma CH_2^{(Ax)}$
16	1265	/	1279	1263(−2)	/	1278	1259(−6)	/	1269	$\nu\ N\text{-}NO_2^{(Ax)} + \gamma CH_2^{(Ax)}$
17	1232	/	1248	1220(−12)	/	1236	1201(−31)	/	1246	ν N–C–N
18	1214	1217		1209(−7)	1210(−7)	1207	/	1200(−17)	1206	ν N–C–N
19	1037	1031	1027	1031(−6)	1025(−6)	1015	1025(−12)	1016(−15)	1013	ν N–C–N
20	1016	/	1003	1006(−10)	/	996	1008(−8)	/	1000	$\beta\ CH_2^{(Eq)} + \nu\ N\text{-}NO_2$
21	943	945	944	935(−8)	935(−10)	934	937(−6)	936(−9)	942	$\beta\ CH_2^{(Eq)} + \nu\ N\text{-}NO_2$
22	919	/	903	900(−19)	/	891	914(−4)	/	900	$\gamma\ CH_2$
23	881	884	890	863(−18)	866(−19)	876	880(−1)	882(−2)	885	rg breathing
24	852	849	865	831(−21)	835(−14)	858	840(−12)	844(−5)	856	ν C–N–C
25	779	788	798	777(−2)	785(−3)	796	773(−6)	777(−11)	793	ν N–C–N
26	/	670			659(−11)	668	/	663(−7)	668	β rg
27	601	606	608	597(−4)	599(−7)	602	599(−2)	602(−4)	606	β rg
28	588	591	587	582(−6)	585(−6)	579	584(−4)	586(−5)	585	β rg
29	/	463	463	/	458(−5)	461	/	459(−4)	461	β rg
30	/	415	410		411(−4)	401	/	407(−8)	400	β rg
31	/	347	331	/	344(−3)	321		343(−4)	321	γ rg
32	/	226	228	/	226(0)	227	/	220(−6)	228	γ rg
33	/	153	/	/	153(0)	/	/	150(−3)	/	$\gamma\ NO_2$

The numerical values in parenthesis are the isotopic shift of frequencies.

[a] Calculated with B3LYP/6-3411++G**; scaled according to correlation equation $\nu_{obs}/\nu_{calc} = 1.0087(9) - 0.0000163(6)(\nu_{calc}/cm^{-1})$.

[b] Vibrational modes: ν, stretching; β, bending in plane; γ, bending out-of-plane; rg, ring; superscript s, symmetric; superscript as, asymmetric; superscript Ax, axial; superscript Eq, equatorial.

[c] Estimated graphical representation.

to be detected because they are either too weak or appear below the limit of detection in this study. The assignments for the IR and Raman frequencies of α-RDX and its isotopomers, together with the results of the B3LYP calculations are listed in Table 1. The problem of the overestimation of frequencies, commonly encountered in DFT vibrational frequencies calculations due to the neglecting of anharmonicity effects, was solved using a wavenumber-linear scaling (WLS) method [22] with the following relationship:

$$\frac{\nu_{obs}}{\nu_{calc}} = 1.0087(9) - 0.0000163(6)(\nu_{calc}/\mathrm{cm}^{-1}) \quad (1)$$

All assignments were determined by comparison of experimental shifted data of the labeled RDX with the calculated wavenumbers and vibrational modes at each selected mode. There are some differences of wavenumbers between calculated and experimental data. This is due to the fact that the calculated spectra correspond to the gas phase whereas experimental data are taken with solid RDX. However, the spectral patterns are similar. The assignments of selected normal vibrations of the RDX, $^{13}C_3$- and $^{15}N_3$-RDX isotopomers are presented in Table 1, listing the experimental and the calculated frequencies. The mode number assignments (indicated in parenthesis in the following discussion) are made from comparisons of experimental spectra and theoretical calculations. Very weak signals were not labeled. The calculation gives a reasonable prediction of the normal mode frequencies and the observed isotopic shifts. The normal harmonic frequencies tend to become smaller with increasing isotopic mass, and intensities sometimes change.

4.1. C–H vibrations

4.1.1. C–H vibrations stretching (ν_{C-H}) vibrations

Four medium intensity Raman bands observed in the region from 2800 to 3200 cm^{-1} were readily assigned to asymmetric stretching modes (ν). The two bands at 3076(1) and 3067(2) were assigned to C–H equatorial asymmetric stretching modes ($\nu^{as}C\text{–}H^{(Eq)}$). The bands at 2995(3) and 2949 cm^{-1} (4) were attributed to asymmetric stretching mode of the C–H axial group ($\nu^{as}C\text{–}H^{(Ax)}$). Only the former two are observable in infrared spectra. The change from ^{12}C to ^{13}C decreased the frequencies in this spectral region by 10 cm^{-1}. Fig. 4 shows the experimental Raman spectra for RDX and isotopomers from 100 to 1700 cm^{-1}.

4.1.2. In-plane C–H bending (β_{C-H}) vibrations

The infrared bands corresponding to the C–H in plane bending vibrations are observed at 1457(8) and 1430 cm^{-1} (9). The respective Raman bands were located at 1459 and 1436 cm^{-1}. Modes 9 and 8 are attributed to β-CH_2 equatorial and axial group, respectively, in both IR and Raman spectra, and were downshifted by 4.0 cm^{-1} as isotopic mass of the methylene increased. The band at 919 cm^{-1} (22) in the IR spectra is also assigned to this vibration.

4.1.3. Out-of-plane C–H bending (γ_{C-H}) vibrations

The C–H out-of-plane (γ) modes appeared as a series of three medium intensity bands (10-12). The band at 1421 cm^{-1} (10) was observed in the IR spectra only and corresponds to equatorial γ_{C-H} mode. A combination of axial/equatorial γ_{C-H} modes (11) was observed at 1386 cm^{-1} in IR and Raman spectra. The axial γ_{C-H} mode in Raman spectra, not observed in IR spectra, was identified at 1379 cm^{-1} (12).

4.2. Nitro group vibrations

The NO_2 antisymmetric stretching modes gave rise to characteristics bands observed in both IR and Raman spectra, covering the spectral range from 1520 to 1600 cm^{-1}. The IR bands are 1589(5), 1567(6) and 1527 cm^{-1} (7); the Raman bands are: 1595(5), 1573(6) and 1541 cm^{-1} (7). Of these three signals, two are attributed to axial nitro groups (5,6) and the third to an equatorial nitro group (7). These bands were shifted by 4.0 cm^{-1} in the $^{15}N_3$-RDX isotopomer and remain unaffected by ^{13}C isotopic substitution. In addition, the 153 cm^{-1} (33) band in the Raman spectra of RDX was assigned to the out-of-plane mode of the nitro groups.

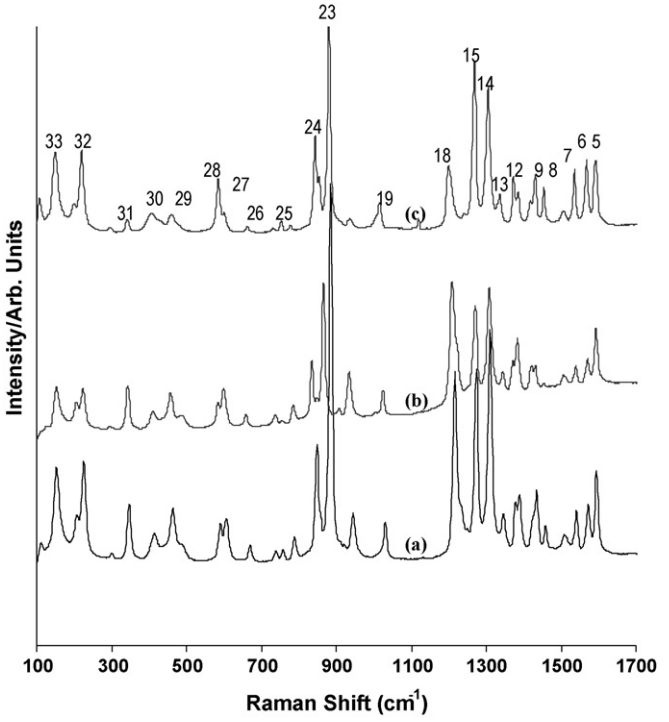

Fig. 4. Experimental Raman spectra for RDX and isotopically labeled RDX from 100 to 1700 cm^{-1}; (a) RDX, (b) $^{13}C_3$-RDX and (c) $^{15}N_3$-RDX. Labeled peaks are explained in Table 1.

4.3. Nitramine N-NO_2 (ν_{N-NO_2}) stretching vibrations

In previous works [1,2] bands at 1348(13) and 1309 cm^{-1} (14) were assigned to combination and out-of-plane bending modes. According to the IR and Raman spectra and comparative shift values for RDX isotopomers, these bands were readily assigned as N-NO_2 stretching modes. Other bands that correspond to these modes of vibration were observed in the Raman spectra at 1275(15) and 945 cm^{-1} (21); and the IR spectra at 1265(16) and 1016 cm^{-1} (20). In all these modes, contributions of in-plane and out-of-plane C–H bending vibration were observed as illustrated in Table 1.

4.4. Ring vibrations

A group of four bands (modes 17, 18, 19 and 25) have been assigned to the stretching N–C–N (ν_{N-C-N}) mode. The 1232 cm^{-1} (17) band in the IR spectra was not observed in Raman spectra. The $^{15}N_3$-labeling of RDX results in a downward shift of 31, 15, 17 and 11 cm^{-1} of these vibrational frequencies, respectively. The most symmetrical normal mode of ring, known as the ring breathing mode (23), was readily assigned to the band at 881 and 884 cm^{-1} in the IR and Raman spectrum, respectively. The 852 cm^{-1} IR band and 849 cm^{-1} (24) Raman band for unlabeled RDX were assigned to the stretching C–N–C bond in the ring (ν_{C-N-C}). This band experienced downward isotopic shifts of 21 (IR) and 14 cm^{-1} (Raman) by $^{13}C_3$-labeling. The in-plane ring bending modes gave rise to weak bands across the low-frequency region, below 1000 cm^{-1}. With the

exception of medium strong IR bands at 601(27) and 588 cm^{-1} (28), a group of weak bands assigned to the 670(26), 591(28), 463(29) and 415 cm^{-1} (30) were only observed in the Raman spectra. The modes remaining (31 and 32) in the 350–200 cm^{-1} region can be associated with the out-of-plane ring modes. The CH_2 bending vibration, does not shift much in energy for $^{13}C_3$ and $^{15}N_3$, revealing the lack of involvement of the triazine ring in these modes. Some of these assignments are in agreement with typical values reported for RDX ring vibrations [5].

5. Conclusions

Infrared and Raman spectra of the cyclic nitramine RDX in the α-phase, and ^{13}C, and ^{15}N (on ring) enriched RDX analogues in the solid state were recorded and their fundamental frequencies have been assigned using isotopic frequency shifts. The IR and Raman spectra for α-RDX and its isotopic derivatives were also computed using density functional calculations and compared with the normal isotopic experimental spectra. The results of the calculations were in reasonable agreement with the observed wavenumber locations, in most of the cases. DFT calculations have also allowed more definitive set of assignments to be made for α-RDX and its isotopomers. The experimental results obtained in this study for RDX, $^{13}C_3$- and $^{15}N_3$-RDX compared with theoretical data allowed deriving correlations of observed frequency deviations of certain vibration modes and the effect of isotopic substitution on the RDX molecule. Most of the observed vibrational bands have been successfully assigned by the present work.

Acknowledgments

This work was supported by the U.S. Department of Defense, University Research Initiative Multidisciplinary University Research Initiative (URI)-MURI Program, under grant number DAAD19-02-1-0257. The authors also acknowledge contributions from Aaron LaPointe of Night Vision and Electronic Sensors Directorate, Department of Defense. We also thank the Chemical Imaging Center of the Department of Chemistry of University of Puerto Rico-Mayagüez for the financial support of this project.

Support from the U.S. Department of Homeland Security under Award Number 2008-ST-061-ED0001 is also acknowledged. However, the views and conclusions contained in this document are those of the authors and should not be interpreted as necessarily representing the official policies, either expressed or implied, of the U.S. Department of Homeland Security.

References

[1] A. Filhol, C. Clement, M.T. Forel, J. Pavot, M. Rey-Lafon, G. Richoux, C. Trinquecoste, J. Cherville, J. Phys. Chem. 13 (1971) 2056–2059.
[2] R.J. Karpowicz, T.B. Brill, J. Phys. Chem. 88 (1984) 348–352.
[3] R. Infante, S.P. Hernandez, Proc. SPIE 6201 (2006) 62012F1–62018F.
[4] N.J Harris, K. Lammertsma, J. Am. Chem. Soc. 119 (1997) 6583–6589.
[5] B.M. Rice, C.F. Chabalowski, J. Phys. Chem. 101A (1997) 8720–8726.
[6] B.M. Rice, T. Vladimiroff, J. Phys. Chem. 106A (2002) 10437–10443.
[7] L. Pacheco, O. Primera, M. Ramirez, O. Ruiz, S.P. Hernandez, Proc. SPIE 6206 (2006) 34–38.
[8] D.G. Hallis, J. Axel, P.F. Taday, T.M. Korter, Chem. Phys. Lett. 463 (2008) 84–89.
[9] W. McCrone, Anal. Chem. 22 (1950) 954.
[10] C. Choi, E. Prince, Acta Crystallogr. Sect. B 28 (1972) 2857–2862.
[11] R.J. Karpowicz, S.T. Sergio, T.B. Brill, Ind. Eng. Chem. Prod. Res. Dev. 22 (1983) 363–365.
[12] P. Torres, I. Cotte, S.P. Hernandez, N. Mina, A. Santana, R. Chamberlain, R. Lareau, M. Castro, J. Phys. Chem. B 108 (2004) 8799–8805.
[13] N. Goto, H. Fujihsia, H. Yamawaki, K. Wakabayashi, Y. Nakayama, M. Yoshida, M. Koshi, J. Phys. Chem. B 110 (2006) 23655–23659.
[14] Z.A. Dreger, Y.M. Gupta, J. Phys. Chem. B 111 (2007) 3893–3903.
[15] J.E. Patterson, Z.A. Dreger, Y.M. Gupta, J. Phys. Chem. B 111 (2007) 10897–10904.
[16] J.A. Ciezak, T.A. Jenkins, Z. Liu, R.J. Hemley, J. Phys. Chem. A 111 (2007) 59–63.
[17] W. Kohn, A.D. Becke, R.G. Parr, J. Phys. Chem. 100 (1996) 12974–12980.
[18] M.J. Frisch, G.W. Trucks, H.B. Schlegel, G.E. Scuseria, M.A. Robb, J.R. Cheeseman, V.G. Zakrzewski, J.A. Montgomery Jr., R.E. Stratmann, J.C. Burant, S. Dapprich, J.M. Millam, A.D. Daniels, K.N. Kudin, M.C. Strain, O. Farkas, J. Tomasi, V. Barone, M. Cossi, R. Cammi, B. Mennucci, C. Pomelli, C. Adamo, S. Clifford, J. Ochterski, G.A. Petersson, P.Y. Ayala, Q. Cui, K. Morokuma, D.K. Malick, A.D. Rabuck, K. Raghavachari, J.B. Foresman, J. Cioslowski, J.V. Ortiz, A.G. Baboul, B.B. Stefanov, G. Liu, A. Liashenko, P. Piskorz, I. Komaromi, R. Gomperts, R.L. Martin, D.J. Fox, T. Keith, M.A. Al-Laham, C.Y. Peng, A. Nanayakkara, C. Gonzalez, M. Challacombe, P.M.W. Gill, B.G. Johnson, W. Chen, M.W. Wong, J.L. Andres, M. Head-Gordon, E.S. Replogle, J.A. Pople, GAUSSIAN 03 (Revision A.9), Gaussian, Inc., Pittsburgh, 2003.
[19] C. Lee, W. Yang, R.G. Parr, Phys. Rev. B37 (1988) 785–789.
[20] A.D. Becke, J. Chem. Phys. 98 (1993) 5648–5652.
[21] A. Frisch, R.D. Dennington, T.A. Keith, A.B. Nielsen, A.J. Holder, GaussView 03, Gaussian, Inc., Pittsburgh, 2003.
[22] H. Yoshida, A. Ehara, Chem. Phys. Lett. 325 (2000) 477–483.